An efficient synthesis towards the core of Crinipellin: TD-DFT and docking studies

Article *in* Journal of Saudi Chemical Society · January 2021

DOI: 10.1016/j.jscs.2020.101193

10 authors, including:

Raghaba Sahu
Seoul National University
15 PUBLICATIONS **288** CITATIONS
SEE PROFILE

Ranjan Kumar Mohapatra
Government College of Engineering Keonjhar under Biju Patnaik University of Tec…
322 PUBLICATIONS **3,362** CITATIONS
SEE PROFILE

Saud I. Al-Resayes
King Saud University
230 PUBLICATIONS **5,246** CITATIONS
SEE PROFILE

Debadutta Das
Buxi Jagabandhu Bidyadhar Autonomous College
62 PUBLICATIONS **1,428** CITATIONS
SEE PROFILE

Journal of Saudi Chemical Society (2021) **25**, 101193

King Saud University

Journal of Saudi Chemical Society

www.ksu.edu.sa
www.sciencedirect.com

ORIGINAL ARTICLE

An efficient synthesis towards the core of Crinipellin: TD-DFT and docking studies

Raghaba Sahu [a,*], Ranjan K. Mohapatra [b,*], Saud I. Al-Resayes [c], Debadutta Das [d], Pankaj K. Parhi [e], Shakilur Rahman [f], Lucia Pintilie [g,*], Manjeet Kumar [h], Mohammad Azam [c,*], Azaj Ansari [h,*]

[a] *College of Pharmacy, Seoul National University, Seoul 08826, South Korea*
[b] *Department of Chemistry, Government College of Engineering, Keonjhar, Odisha 758002, India*
[c] *Department of Chemistry, College of Science, King Saud University, PO Box 2455, Riyadh 11451, Saudi Arabia*
[d] *Department of Chemistry, Sukanti Degree College, Subarnapur, Odisha 767017, India*
[e] *Department of Chemistry, Fakir Mohan (F.M.) University, VyasaVihar, Nuapadhi, Balasore 756089, Odisha, India*
[f] *Department of Bioscience, Jamia Millia Islamia, New Delhi 110025, India*
[g] *Department of Synthesis of Bioactive Substances and Pharmaceutical Technologies, National Institute for Chemical & Pharmaceutical Research and Development, Bucharest, Romania*
[h] *Department of Chemistry, Central University of Haryana, Mahendergarh, Haryana 123031, India*

Received 18 October 2020; revised 26 December 2020; accepted 27 December 2020
Available online 7 January 2021

KEYWORDS

Crinipellin;
TD DFT;
Docking study

Abstract In this present report, we are describing a novel route for the synthesis of the tetracyclic ring systems, a common core of crinipellin, via oxidative dearomatization, cycloaddition and oxa-di-pi-methane rearrangement. We are also concerned to explore a route to tetracyclic core (**1e**) of Crinipellin and tricyclic core (**1g**) of Allicaol B through intermolecular diels alder reaction and photochemically 1,2 acyl shift. Moreover, docking study of compound 13 and 16 is investigated against AcrB multidrug efflux pump of *Escherichia coli* (PDB ID: 1T9U), main protease of SARS COV-2 (PDB ID: 6W63), DNA gyrase of *Streptococcus pneumonia* (PDB ID: 4Z2C), human estrogen receptor alpha (PDB ID: 3ERT), human lanosterol 14-alpha-demethylase (CYP51)(PDB ID: 3JUS) and cyclooxygenase-2 (Prostaglandin Synthase-2) (PDB ID: 1CX2). The obtained results are important for the exploitation of the therapeutic potential of these derivatives as antimicrobial,

* Corresponding authors.
E-mail addresses: raghabasahu@gmail.com (R. Sahu), ranjank_mohapatra@yahoo.com (R.K. Mohapatra), lucia.pintilie@gmail.com (L. Pintilie), mhashim@ksu.edu.sa (M. Azam), azaj@cuh.ac.in (A. Ansari).
Peer review under responsibility of King Saud University.

Production and hosting by Elsevier

https://doi.org/10.1016/j.jscs.2020.101193

antiviral, anticancer, antifungal or anti-inflammatory agents. In addition, TD-DFT studies of the compounds are also carried out.

1. Introduction

Polyquinane (natural products) with complex molecular architecture have generated a sustained interest among synthetic chemists owing to wide-ranging biological properties [1–4]. Kupka *et al* described the separation of an antibiotic crinipellin A (**1a**) from the submerged cultures of basidomycete *Crinipellisstipitaria,* strain 7612*,* most active against gram-positive bacteria [5]. After that, some more crinipellins (**1b-d**) (Fig. 1) were also isolated and investigated for their antibiotic activity against various strains of *C. Stipitaria* [6–8]. Crinipellins, are the first group of polyquinane diterpenoids to contain a tetraquinane framework which integrates together a linear cis:anti:cistriquinane along with angular triquinane ring systems. Studies towards synthesis of architecturally more complex crinipellins are limited in literature [9–18]. However, there are some reports on the development of novel approaches for constructing molecular complexity by oxidative dearomatization of *o*-hydroxymethyl phenols, cycloaddition and photochemical reactions [19–23]. Taking into consideration of interest towards crinipellin (**1**) as well as alliacol B (**2**), we extended our previous approach towards angular triquinane [24] to tetraquinane and alliacol B. Herein, we report a novel route for the synthesis of the tetracyclic ring systems (**1e**), which is a common core of crinipellin via oxidative dearomatization, cycloaddition and oxa- di-pi-methane rearrangement. We considered to exploring a route to tetraquinane (**1e),** a core of Crinipellin through intermolecular diels alder reaction and photochemically 1,2 acyl shift (Scheme 1). The detailed synthetic procedure is given in supplementary section. It was contemplated that the angularly fused tetraquinane of type (**1e**) may be obtained from compound (**6**) by cyclopropane ring cleavage followed by hydrogenation. As we are aware that current COVID-19 outbreak driven by the highly

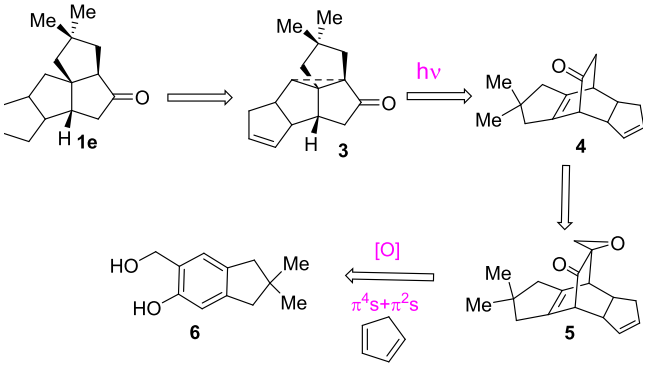

Scheme 1

infectious SARS-CoV-2 caused the present pandemic and emerged as the most critical universal health disaster of this century [25,26]. In this article, we are reporting the molecular docking analyses of the synthesized compounds against selected proteins/enzymes receptors using CLC Drug Discovery Workbench Software. In addition, TD-DFT studies are also recorded for compounds **4**, **5**, **11**, **13,** and **16**.

2. Result and discussion

In continuation of our theme towards the synthesis of angular triquinanes, we also explored a synthetic route to angular tetraquinanes along the similar lines as presented earlier. The tetracyclic chromophoric system (**4**) was readily synthesized from the precursor (**6**). Interestingly, oxidative dearomatization of **6** in the presence of cyclopentadiene directly yielded the adduct **5** in reasonable yield along with some un-reacted spiroepoxycyclohexa-2,5-dienone **9** (Scheme 2). This is pre-

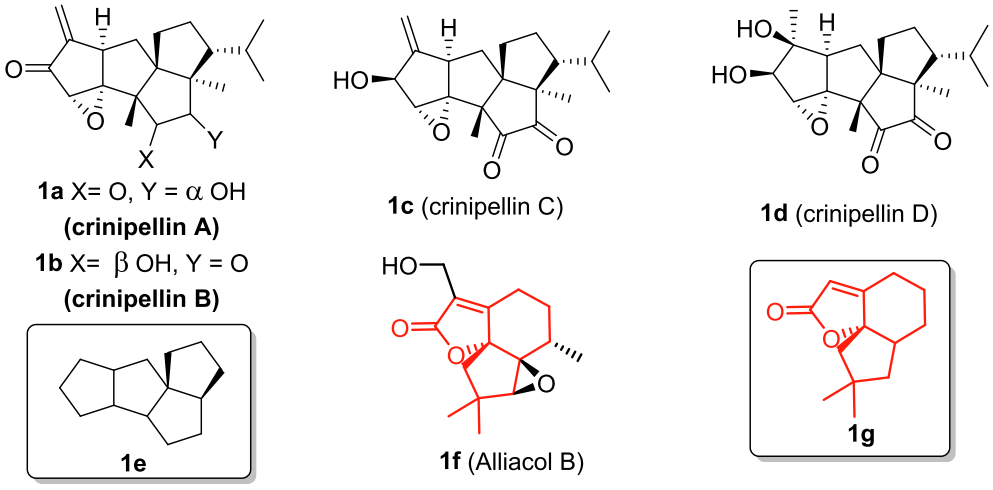

Fig. 1 Structure of some crinipellins.

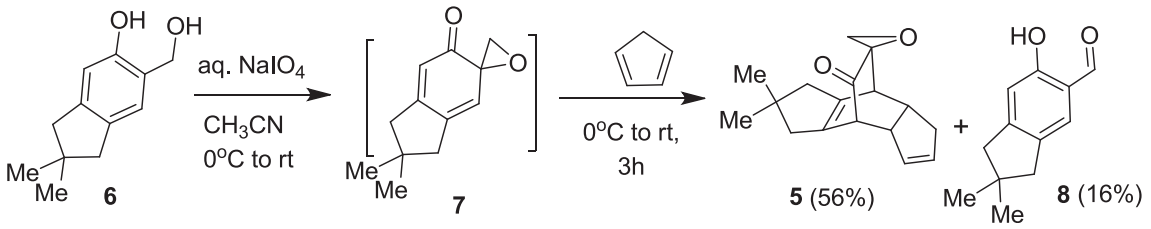

Scheme 2

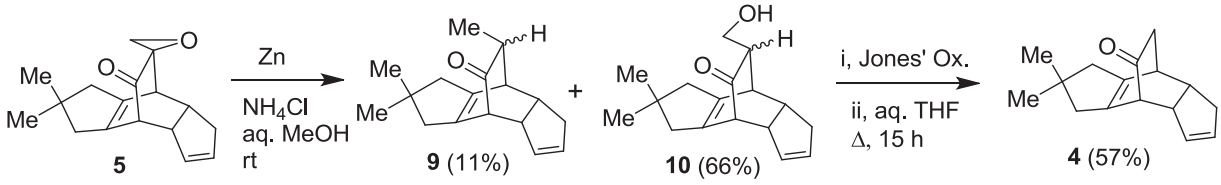

Scheme 3

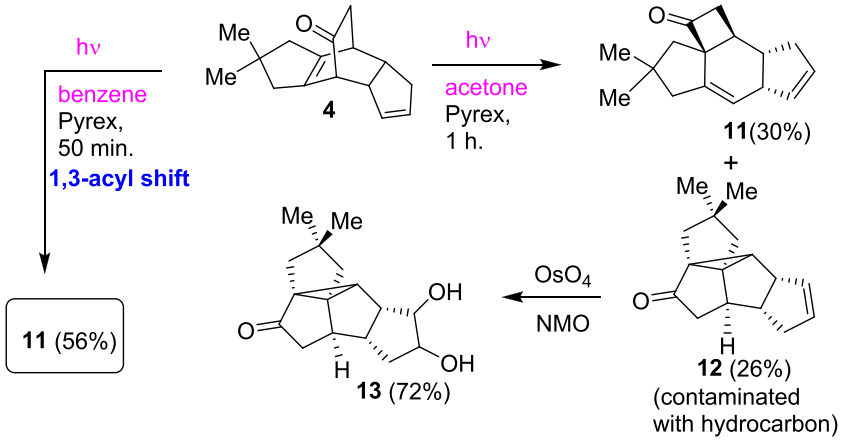

Scheme 4

sumably due to high reactivity of cyclopentadiene which could intercept the cyclohexadienone **9** formed *in situ* even under ambient conditions.

Furthermore, it may be worth noting that adduct **5** is formed in a highly regio- and stereo selective cycloaddition wherein the cyclohexadienone behaves as 4π-partner and cyclopentadiene as a 2 π -partner (dienophile) and that other products arising from alternate pericyclic modes [such as π^4s (cyclopentadiene) + π^2s (cyclohexadienone)] was not formed.

Keto-epoxide **5** was changed to tricyclic compound **4** in good yield (Scheme 3).

Furthermore, the tetracyclic compound **4** was irradiated in acetone to find **11** with cyclobutanone ring formed due to 1,3-acyl shift and pentacyclic compound **12** (formed due to oxa-di-π -methane rearrangement) in almost equal yields (Scheme 4).

The NMR spectra of the nonpolar product **12** indicated that it is contaminated with some inseparable hydrocarbon (which could not be separated even after repeated column chromatography). Therefore, the product **12** was subjected to dihydroxylation with OsO_4 which gave the pentacyclicdiol **13** (Scheme 4) in excellent yield as a single diastereoisomer (^{1}H and ^{13}C NMR spectra) whose structure was fully corroborated with its spectral characteristics. However, stereochemical position of the hydroxyl groups was not easily visible from spectral features.

The behaviour of tetracyclic compound **4** is same with previous tricyclic chromophoric systems **14** under photochemical transformation [24]. Compound **15** was formed as a major amount in both direct irradiation as well as sensitized irradiation of compound **14**, which was converted to its tricyclic lactone **16,** a core of **Alliacol B**. The lactonisation was done by Bayer-Villiger reaction by treating with m-CPBA in the presence of $NaHCO_3$ (Scheme 5) and leads to single regioisomer **16**.

3. Molecular docking studies

Molecular docking study [27] was effectuated on two ligands (studied compounds) to obtain accurate predictions about structure and their interactions with a protein/enzyme receptor in order to evaluate the biological activity. We used proteins/enzymes receptors imported from protein data bank (http://www.rcsb.org/:PDB), AcrB multidrug efflux pump of *Escherichia coli* (PDB ID: 1T9U [28]), main protease of SARS COV-2 (PDB ID: 6W63 [29]), DNA gyrase of *Streptococcus pneumonia*

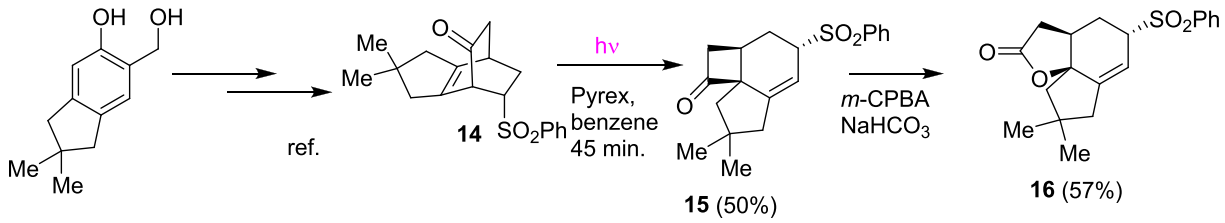

Scheme 5

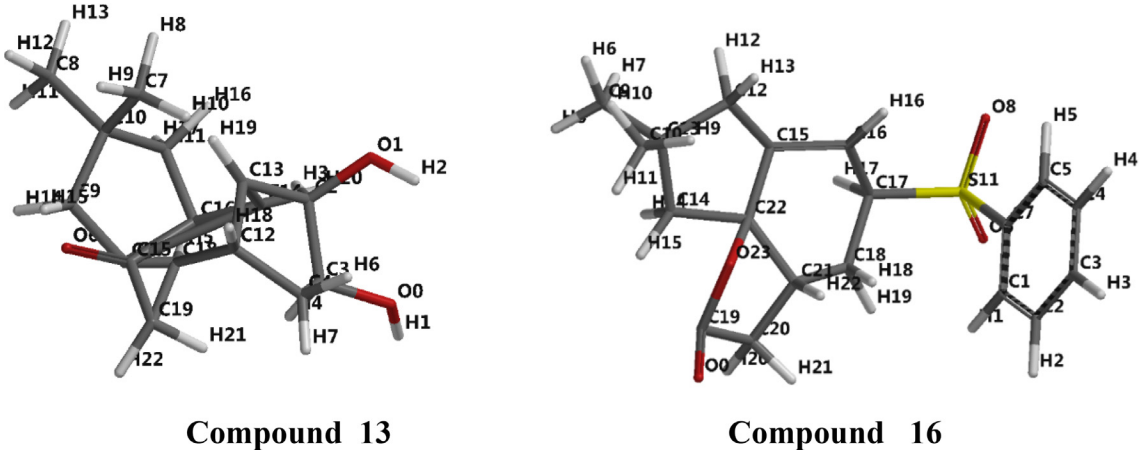

Fig. 2 Tube representation of the optimized molecular structure of compounds **13** and **16** (Numbering of the atoms was done according to the software).

(PDB ID: 4Z2C [30]), human estrogen receptor alpha (PDB ID: 3ERT [31]), human lanosterol 14-alpha-demethylase (CYP51)(PDB ID: 3JUS [32]) and cyclooxygenase-2 (Prostaglandin Synthase-2) (PDB ID: 1CX2 [33].

In the docking simulation, the ligands (compounds **13** and **16**) (Fig. 2) are placed into a predictable binding site on the surface of a protein target. CLC Drug Discovery Workbench also utilizes MMFF94 (MMFF) force field to generate 3D structure on import. Different conformations are generated by rotation about rotatable bonds and conformation changes. Thus, the ligand optimizer was realized by geometry minimization using MMFF94 force field. The minimization of the ligand is conforming to the binding pocket geometry. The protein–ligand interaction is scored, and the best scoring binding mode is returned for individual ligand and collected with the score. The search for the binding mode of the ligand is operated in the binding site (green sphere with a radius large enough to comprise all ligands docked to the receptor protein). After the import of the protein receptor from PDB bank, the next step is the setup binding site and the setup binding pockets; binding pockets are necessary to guide the docking simulation. After the setup, the binding site and pocket, the co-crystallized- natural ligand was extracted and redocked in the active binding site of the protein receptor to validate the method and the docking parameters obtained from the molecular docking studies.

3.1. Docking evaluation against AcrB multidrug efflux pump of Escherichia coli

The docking pose of ciprofloxacin (co-crystallized) interacting with amino acid residues and the hydrogen bonds created with ARG 468 (three bonds: 3.129 Å, 3.062 Å and 3.073 Å) are given in Figure S1a. The docking score of the compounds **13** and **16** are smaller than docking score of co-crystallized (docking score: −46.33; RMSD: 0.67 Å). The compound **16** has a docking score: −46.33 (RMSD: 0.67 Å), and shows occurence of three hydrogen bonds, one with GLN 469 (2.631 Å) and two with ARG 468 (2.620 Å and 3.112 Å) (Fig. 3a). The compound **13** showed occurence of six hydrogen bonds with ARG 468 (2.884 Å), ASN 391 (3.290 Å), GLY 387 (3.219 Å) and three with SER 389 (2.466 Å, 2.918 Å, and 3.158 Å) (Figure S2a). The docking pose of the co-crystallized CPX and of the compounds **13** and **16** interacting with the amino acids residues is presented in Figure S1b, 3b and S2b. The amino acids residues that formed the interacting group of each ligand are listed in Table S1. After analyzing the data obtained from the docking study, it was observed that the two studied compounds were placed in the same binding site of 1T9U as the cocrystallized one (Fig. 3c).

3.2. Docking evaluation against main protease (M^{pro}) of SARS-CoV-2

The docking pose of X77 (co-crystallized) interacting with amino acid residues and the hydrogen bonds created with GLU 166 (2.721 Å) and GLY 143(3.202 Å) are shown in Figure S3a. The co-crystallized X77 **(**N-(4-*tert*-butylphenyl)-N-[(1R)-2-(cyclohexylamino)-2-oxo-1-(pyridin-3-yl)ethyl]-1H-imidazole-4-carboxamide**)** was taken as reference to compare the docking results of the compounds **16** and **13**. The docking score of the compound **16** (docking score: −56.15; RMSD: 0.11 Å) is close to that of the co-crystallized (docking score:

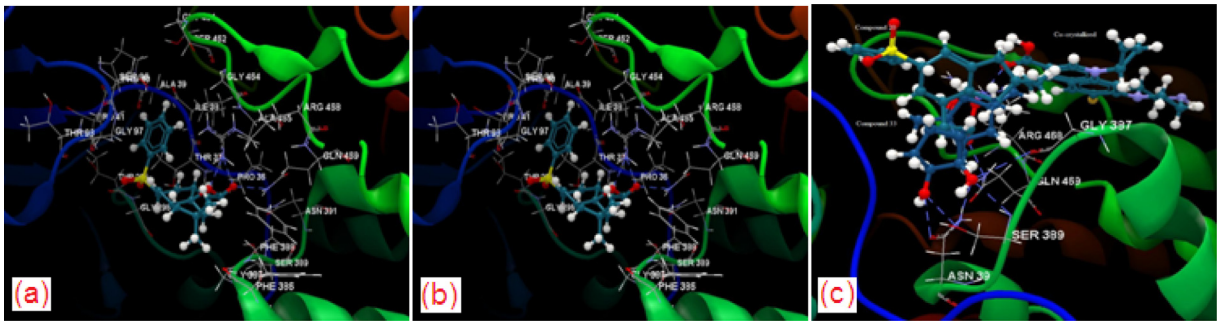

Fig. 3 **(a)** Hydrogen bonds (blue dotted lines) between Compound **16** and ARG 468 GLN 469 amino acids**, (b)** Docking pose of compound **16** interacting with the amino acid residues of binding site of 1T9U**, (c)** Docking pose of the co-crystallized CPX and compounds **16** and **13** in the binding site of 1T9U.

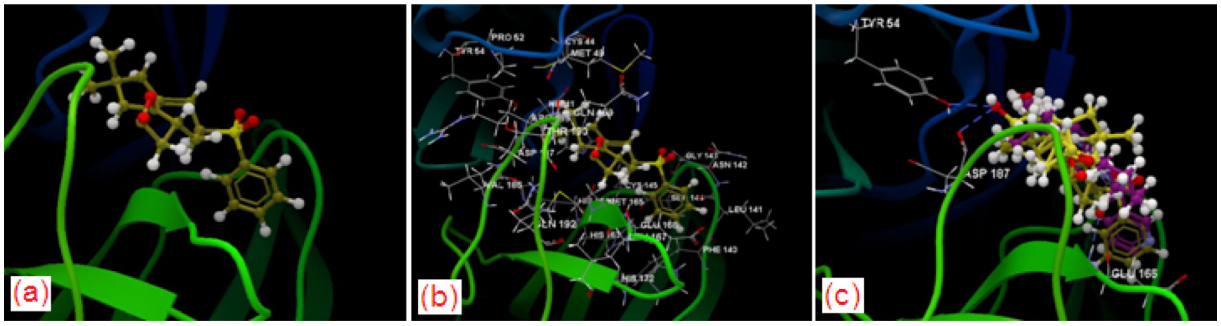

Fig. 4 **(a)** Doching pose of compound **16**, (b) Docking pose of compound **16** interacting with the amino acid residues of the binding site of 6W63, (c) Docking pose of the co-crystallized (purple) and compound **16** (olive) and **13** (yellow) in the binding site of 6W63.

−56.57; RMSD: 1.53 Å), but these compound do not realize hydrogen bonds with the amino acids of the active site of the protein receptor (Fig. 4a). Compound **13** shows occurence of two hydrogenbonds with TYR 54 (2.765 Å) and ASP 187 (2.752 Å) (Figure S4a). The docking pose of the co-crystallized and compounds **16** and **13** interacting with the amino acids residues is presented in Figure S3b, 4b and S4b. The amino acids residues formed the interacting group of each ligand are listed in Table S2. After analyzing the data obtained from the docking study, it was observed that the two studied compounds were placed in the same binding site of 1T9U as the cocrystallized one (Fig. 4c).

3.3. Docking evaluation against Streptococcus pneumoniae DNA gyrase

Figure S5a shows the docking pose of co-crystallized moxifloxacin (MFX) interacting with amino acid residues and nucleotids of the active site and the hydrogen bonds created with SER 436:D (2.953 Å, 3.030 Å, 2.597 Å), DG 1:H (3.099 Å) and DA 2:H (3.112 Å). The docking score of the two compounds **13** and **16** are smaller than docking score of co-crystallized (docking score: −83.33; RMSD: 1.53 Å). The compound **16** has a docking score: −63.48 (RMSD: 0.04 Å) and showed occurence of two hydrogen bonds, one with GLY 457:D (3.096 Å) and with DG 1:H (2.898 Å) (Fig. 5a). The compound **13** showed occurence of four hydrogen bonds with ARG 456:D (3.084 Å), GLU 475:D (2.791 Å), and two with DA 5:F (3.015 Å, 3.133 Å) (Figure S6a). The docking pose of the co-crystallized and of the compounds **16** and **13** interacting with the amino acids residues is presented in Figure S5b, 5b and S6b. The amino acids residues that formed the interacting group of each ligand are listed in Table S3. After analyzing the data obtained from the docking study, it was observed that the two studied compounds were placed in the same binding site of 4Z2C as the cocrystallized one (Fig. 5c).

3.4. Docking evaluation against human estrogen receptor alpha

Figure S7a shows the docking pose of 4-hydroxytamoxifen (co-crystallized OHT) interacting with amino acid residues of the active site and the hydrogen bonds created with GLU 353 (2.998 Å) and ARG 394 (2.397 Å). However, the docking score **13** and **16** are smaller than docking score of co-crystallized (docking score: −76.36; RMSD: 0.68 Å). The compound **16** has a docking score: −54.09 (RMSD: 0.03 Å) and showed occurence of one hydrogen bond with THR 347 (2.742 Å) (Fig. 6a). The compound **13** showed occurence of five hydrogen bonds with ALA 350 (3.311 Å), ARG 394 (3.050 Å), and three with GLU 353 (2.579 Å, 2.586 Å and 3.386 Å) (Figure S8a). The docking pose of the co-crystallized and **16** and **13** interacting with the amino acids residues are presented in Figure S7b, 6b and S8b. The amino acids residues that formed the interacting group of each ligand are listed in Table S4. After analyzing the data obtained from the docking study, it was observed that the two studied compounds were placed in the same binding site of 3ERT as the cocrystallized one (Fig. 6c).

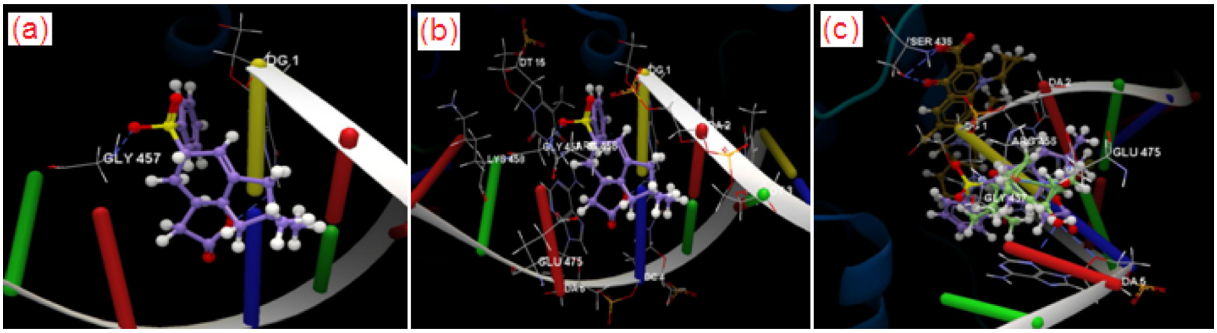

Fig. 5 **(a)** Hydrogen bonds (blue dotted lines) between compound **16** and GLY 457(D) amino acid and DG1(H) nucleotid, **(b)** Docking pose of **16** interacting with the amino acid residues and nucleotids of binding site of 4Z2C, **(c)** Docking pose of co-crystallized (brown) and compound **16** (violet) and **13** (light green) in the binding site of 4Z2C.

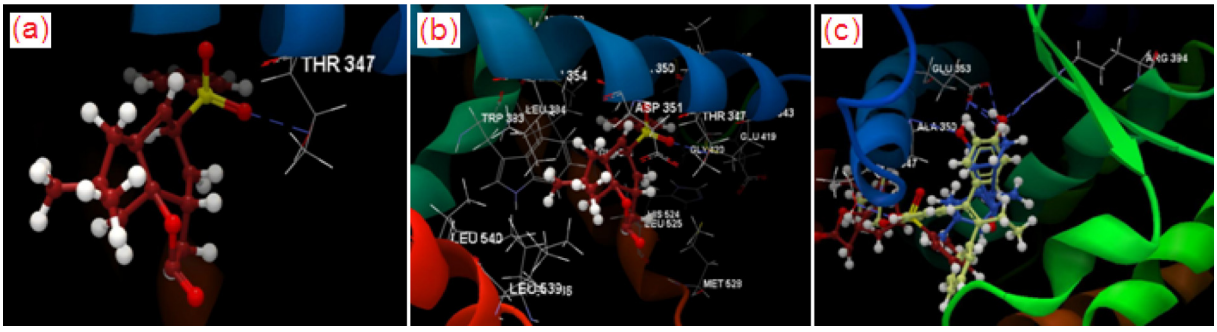

Fig. 6 **(a)** Hydrogen bonds (blue dotted lines) between compound **16** and THR 347 amino acid, **(b)** Docking pose of compound **16** interacting with amino acid residues of binding site of 3ERT, **(c)** Docking pose of the co-crystallized (yelow) and compound **16** (red) and **13** (blue) in the binding site of 3ERT.

3.5. Docking evaluation against human lanosterol 14-alpha-demethylase (CYP51)

Both the ligand (compound 16 and 13) and protein targets were docked on the crystal structure of Cyclooxygenase-2 (Prostaglandin Synthase-2) (PDB ID: 1CX2. The docking pose of co-crystallized ECN interacting with amino acid residues and the hydrogen bond created with TYR 145 (3.103 Å) are given in Figure S9a. The docking score of **16** and **13** are smaller than docking score of co-crystallized (docking score: −84.04; RMSD: 0.93 Å). The compound **16** has a docking score: −70.81 (RMSD: 0.02 Å) and showed occurence of one hydrogen bonds TYR 145 (2.983 Å) (Fig. 7a). The docking studies revealed that the docking score of the compound **13** is −56.78, (RMSD: 0.02 Å) but this compound does not realize hydrogen bonds with the amino acids from the active site of the protein receptor (Figure S10a). The docking pose of the co-crystallized and of the compounds **16** and **13** interacting with the amino acids residues is presented in Figure S9b, 7b and S10b. The amino acids residues that formed the interacting group of each ligand are listed in Table S5. After analyzing the data obtained from the docking study, it was observed that

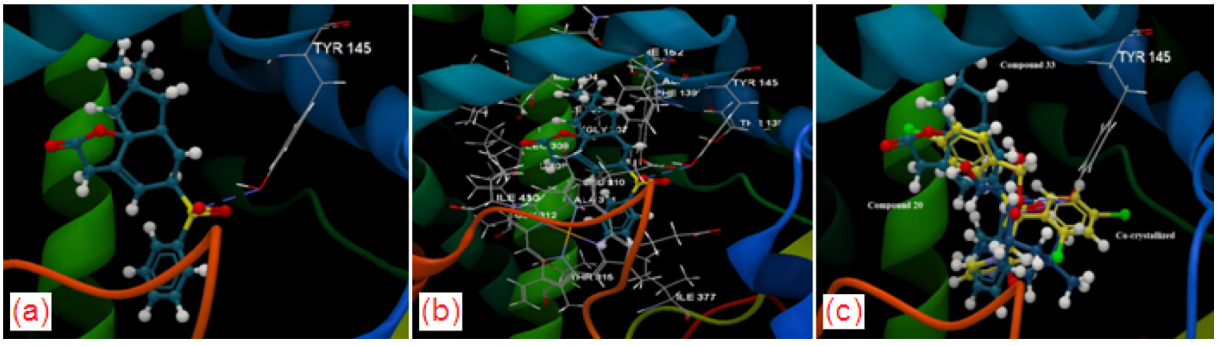

Fig. 7 **(a)** Hydrogen bonds (blue dotted lines) between compound **16** and TYR 145 amino acid, **(b)** Docking pose of **16** interacting with the amino acid residues of binding site of 3JUS, **(c)** Docking pose of the co-crystallized and compounds **16** and **13** in the binding site of 3JUS.

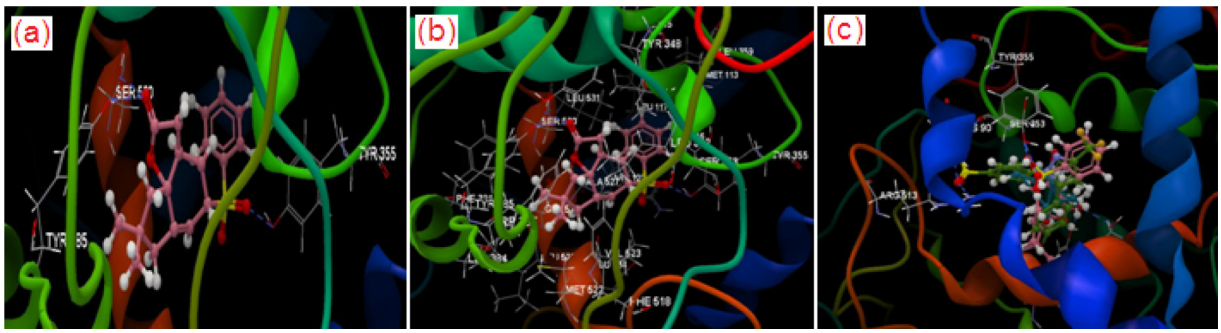

Fig. 8 **(a)** Hydrogen bonds (blue dotted lines) between compound **16** and SER 539, TYR 385 and TYR 355 amino acids, **(b)** Docking pose of compound **16** interacting with the amino acid residues of binding site of 1CX2, **(c)** Docking pose of the co-crystallized (green) and compound **16** (pink) and **13** (ocean blue) in the binding site of 1CX2.

Table 1 Calculated properties of compounds.

Compounds	Atoms	Weight [Daltons]	Flexible bonds	Lipinski violations	Hydrogen donors	Hydrogen acceptors	Log P
Co-crystallized*Cp	42	331.34	3	0	2	6	0.84
Co-crystallized**X77	66	458.58	7	0	1	7	4.59
Co-crystallized***MXF	53	401.43	4	0	2	7	1.62
Co-crystallized****OHT	58	387.51	8	1	1	3	6.78
Co-crystallized*****ECN	39	381.68	6	0	0	3	4.70
Co-crystallized******S58	37	446.24	4	0	2	5	3.65
Compound **16**	46	346.44	2	0	0	4	2.10*/2.75**/2.62*** /1.97****2.22*****/2.62******
Compound **13**	41	262.34	0	0	2	3	0.99

* PDB ID: 1T9U; ** PDB ID: 6 W63; *** PDB ID: 4ZDC; **** PDB ID: 3ERT; ***** PDB ID: 3JUS; ******PDB ID: 1CX2.

the two studied compounds were placed in the same binding site of 3ERT as the cocrystallized one (Fig. 7c).

3.6. Docking evaluation against Cyclooxygenase-2 (Prostaglandin Synthase-2)

Compounds **13** and **16** were docked on the crystal structure of Human lanosterol 14-alpha-demethylase (CYP51) (PDB ID: 1CX2). The docking pose of the co-crystallized S58 (1-phenyl sulfonamide-3-trifluoromethyl-5-*para* bromophenylpyrazole) interacting with amino acid residues and the hydrogen bonds created with HIS 90 (2.894 Å and 3.144 Å), ARG 513 (3.035 Å) and SER 353 (2.534 Å) are displayed in Figure S11a. The docking score of **13** and **16** are smaller than docking score of co-crystallized (docking score: −80.94; RMSD: 0.04 Å). The compound **16** has a docking score: −71.73 (RMSD: 0.04 Å) and showed occurence of three hydrogen bonds, one with SER 530 (2.876 Å) and two with TYR 385 (2.882 Å and 3.091 V Å) (Fig. 8a). **13** showed occurence of one hydrogen bond with TYR 355 (2.872 Å). (Figure S12a). The docking pose of the co-crystallized and of compounds **16** and **13** interacting with the amino acids residues is presented in Figure S11b, 8b and S12b. The amino acids residues that formed the interacting group of each ligand are listed in Table S6. After analyzing the data obtained from the docking study, it was observed that the two studied compounds were placed in the same binding site of 3ERT as the cocrystallized one (Fig. 8c).

On the basis of calculated parameters of Lipinski's rule of five (Table 1), it can be predicted that that molecule with certain properties can turn into an active drug [34]. Furthermore, number of violations evaluate the drug likeness for the molecule. However, it was observed that compounds 13 and 16 have zero violation of all the parameters involved in Lipinski's rule (Lipinski violation is 0). After analyzing the results of the molecular docking study, it is observed that the compounds **13** and **16** possess properties that can turn them into future oral drugs (Lipinski violation is 0) (Table 1). It was also found that compound **16** could be a drug with antimicrobial, antiviral, anticancer, antifungal or anti-inflammatory activity. For all molecular docking studies against the studied targets, it was also observed that compound **16** has a higher docking score than compound **13** and is close to each co-crystallized ligand taken as reference (Fig. 9).

4. Computational details

The time-dependent density functional theory (TD-DFT) calculations were performed using the hybrid B3LYP functional, which is a mixture of exact (HF) and DFT exchange utilizing the B3 functional with the LYP correlation functional [35,36] in combination with the def2-TZVP basis set [37]. In addition, we also employed the resolution-of-identity (RI) approximation technique RIJCOSX to accelerate TD-DFT calculations [38], modulating the chain of spheres (COSX) approximation for the HF exchange term with the Split-RI-J method for the

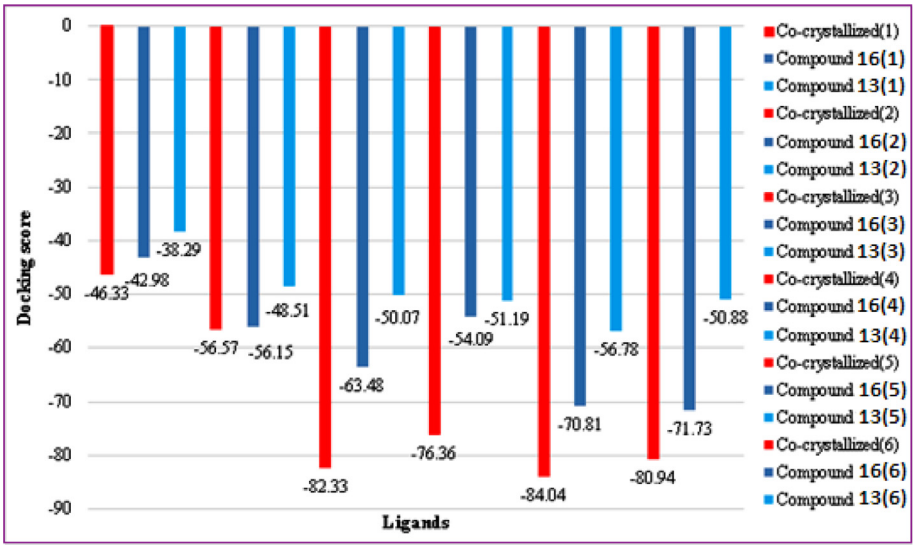

Fig. 9 Docking scores of ligands, (1) PDB ID: 1T9U; (2) PDB ID: 6 W63; (3) PDB ID: 4ZDC; (4) PDB ID: 3ERT; (5) PDB ID: 3JUS; (6) PDB ID: 1CX2.

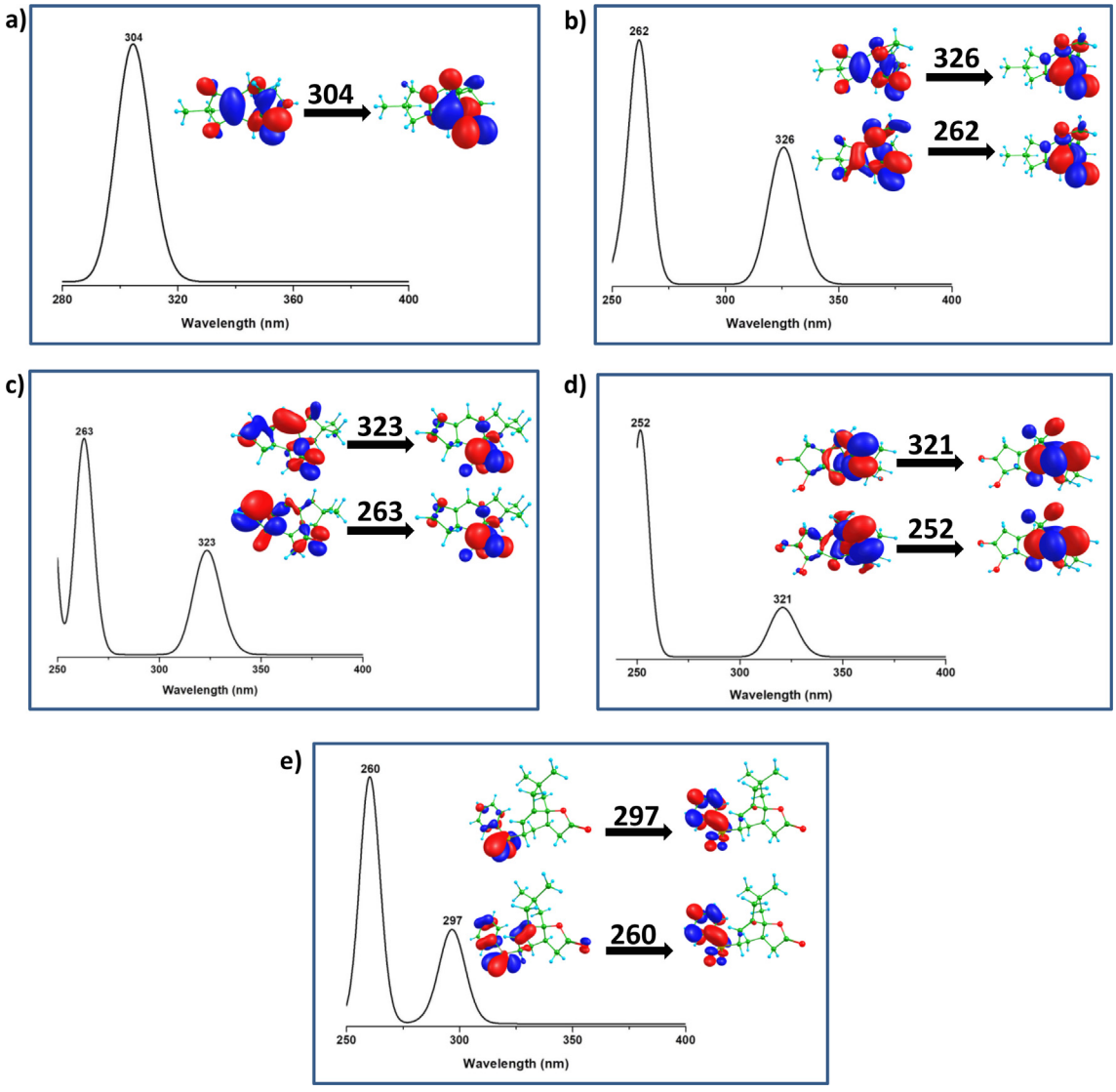

Fig. 10 B3LYP TD-DFT simulated electronic absorption spectra of the compound, a) **11,** b) **5,** c) **4,** d) **13** and e) **16** with their corresponding orbitals involved in their electronic transitions.

Coulomb integrals. The Zeroth-order regular approximation (ZORA) [39–41] was also taken into account to calculate the relativistic effects. All these computations were carried out on the ORCA (*version 4.2.0*) program [42] package using tight SCF convergence criteria and increased integration grids (Grid5).

4.1. TD-DFT study

We have successfully carried out TD-DFT computations to explore the electronic adsorption transitions of five synthesized compounds (**4**, **5**, **11**, **13,** and **16**), which contain heteroatoms, such as S and O in their core structures, generally responsible for π-π* and n-π* electronic transitions. Electrons present in the non-bonding orbital poorly overlap with the π* orbital. As electron pair in n-orbital of heteroatoms have higher energy, and required low energy for the excitation. Therefore, the charge transfer occurring through n-π* transitions generally take place at higher wavelength. In contrast, π to π* orbitals effectively overlap and energy requirements are high for the charge transfer between them. Such transitions (π-π*) occur at a lower wavelength.

Furthermore, we got one intense peak at 304 nm in compound **11,** which reveals the intra ligand charge transfer (ILCT) transition (Fig. 10a) corresponding to π-π* type of electronic transition. In this, an electron can get excitation from a π-bonding to a π*-antibonding orbital. In addition, the orbital involvement is observed from oxygen bonding (p_z) to antibonding (p_x) orbital in this transition. Moreover, charge accumulated on carbonyl carbon atom further suggests the π-π* electronic transition. We got two computed peaks in compound **5** at 262 and 326 nm (Fig. 10b), corresponding to the ILCT transition. However, the more intense peak is observed at 262 nm and shows π-π* transition whereas the lower intense peak at 326 nm exhibits n-π* transition. Similar to compounds **11** and **5**, we also found two peaks at 263 and 323 nm in compound **4**. Among both these peaks, 263 nm peak have more intensity compared to 323 nm peak, and charge accumulation is found more in the π* antibonding orbitals of the carbonyl group (Fig. 10c). The peak observed at 263 nm and 323 nm suggests π-π* and n-π* charge transfer transition respectively. We have also noticed two peaks at 252 and 321 nm in compound 13. The intense peak occurring at 252 nm indicate the π-π* while the peak at 321 nm resemble the n-π* charge transfer transition (Fig. 10d). Next, compound **16** displays two peaks at 260 and 297 nm. However, the first peak has more intensity in comparison to second one. In this compound, the major charge is accumulated on the phenyl ring. Nevertheless, both the peaks show the π-π* charge transfer transition (Fig. 10e).

5. Conclusion

In summary, we have described a facile route to complex molecular skeleton of crinipellin from simple aromatic compound through a short and efficient synthetic route. The sensitized irradiation of **4** led to oxa-di- π -methane reaction only to a moderate extent, thus limiting its synthetic application. Nevertheless, the present study provides additional examples of photoreaction of rigid β,γ-enones and demonstrates the effect of structure on the photoreactivity and provides novel carbocyclic systems, which are not readily accessible otherwise. Moreover, it is observed from molecular docking study that compounds **13** and **16** possess properties that can turn them into future oral drugs. It was also found that compound **16** could be a drug with antimicrobial, antiviral, anticancer, antifungal or anti-inflammatory activity. In addition, compound **16** has a higher docking score than compound **13** and is close to each co-crystallized ligand taken as reference.

Declaration of Competing Interest

The authors declare that they have no known competing financial interests or personal relationships that could have appeared to influence the work reported in this paper.

Acknowledgements

The authors acknowledge the financial support through Researchers Supporting Project number (RSP-2020/147), King Saud University, Riyadh, Saudi Arabia.

Appendix A. Supplementary material

Supplementary data to this article can be found online at https://doi.org/10.1016/j.jscs.2020.101193.

References

[1] L.A. Paquette, A.M. Doherty, Recent Synthetic Developments in Polyquinane Chemistry, Springer-verlag, New York, 1987 and references therein.
[2] G. Mehta, A. Srikrishna, Chem. Rev. 97 (1997) 671 and references therein.
[3] V. Singh, B. Thomas, Tetrahedron 54 (1998) 3647.
[4] H.-Y. Lee, Acc. Chem. Res. 48 (2015) 2308.
[5] J. Kupka, T. Anke, F. Oberwinkler, G. Schramm, W. Steglich, J. Antibiot. 32 (1979) 130.
[6] Y.-Y. Li, Y.-M. Shen, Helv. Chim. Acta 93 (2010) 2151.
[7] T. Anke, J. Heim, F. Knoch, U. Mocek, B. Steffan, W. Steglich, Angew. Chem., Int. Ed. Engl. 24 (1985) 709.
[8] T. King, K. Farrell, T. Halsall, V. Thaller, J. Chem. Soc., Chem. Commun. 20 (1977) 727.
[9] C.E. Schwartz, D.P. Curran, J. Am. Chem. Soc. 112 (1990) 9272.
[10] G. Mehta, K.S. Rao, Reddy, M.S., J. Chem. Soc. Perkin I (1991) 693 and references therein.
[11] P. Chen, P.J. Carroll, S.M. Sieburth, Org. Lett. 12 (2010) 4510.
[12] A. Srikrishna, V. Gowri, Synlett (2011) 2652.
[13] A. Srikrishna, V. Gowri, Tetrahedron 68 (2012) 3046.
[14] E. Piers, J. Renaud, J. Org. Chem. 58 (1993) 11.
[15] E. Piers, J. Renaud, S.J. Rettig, Synthesis (1998) 590.
[16] P.A. Wender, T.M. Dore, Tetrahedron Lett. 39 (1998) 8589.
[17] T. Kang, S.B. Song, W.-Y. Kim, B.G. Kim, H.-Y. Lee, J. Am. Chem. Soc. 136 (2014) 10274.
[18] T. Kang, S.B. Song, H.Y. Lee, J. Am. Chem. Soc. 136 (2014) 10274.
[19] R. Sahu, V. Singh, J. Org. Chem. 82 (2017) 6268.
[20] T.K. Behera, D.B. Jarhad, S.M. Mobin, V. Singh, Tetrahedron 72 (2016) 5377.
[21] R. Sahu, V. Singh, Synthesis 51 (2019) 1633.
[22] V. Singh, B.C. Sahu, V. Bansal, S.M. Mobin, Org. Biomol. Chem. 8 (2010) 4472.
[23] V. Singh, Synlett (2013) 2641.
[24] R. Sahu, V. Singh, Tetrahedron 82 (2017) 6515.

[25] R.K. Mohapatra, P.K. Das, V. Kandi, Diabet. Metabol. Syndrom.: Clin. Res. Rev. 14 (2020) 1593–1594.
[26] R.K. Mohapatra, L. Pintilie, V. Kandi, et al, Chem. Biol. Drug Des. 96 (2020) 1187–1208.
[27] CLC Drug Discovery Workbench, available from http://www.clcbio.com.
[28] E.W. Yu, J.R. Aires, G. McDermott, H. Nikaido, A periplasmic drug-binding site of the AcrB multidrug efflux pump: a crystallographic and site-directed mutagenesis study, JB 187 (19) (2005) 6804–6815, https://doi.org/10.1128/JB.187.19.6804-6815.2005.
[29] A.D. Mesecar, A taxonomically-driven approach to development of potent, broad-spectrum inhibitors of coronavirus main protease including SARS-CoV-2 (COVID-19) (2020), DOI: 10.2210/pdb6W63/pdb, to be published.
[30] I. Laponogov, D.A. Veselkov, X.-S. Pan, J. Selvarajah, I.M.-T. Crevel, L.M. Fisher, M.R. Sanderson, Quinolone (Moxifloxacin)-DNA cleavage complex of gyrase from S. pneumonia (2020) DOI: 10.2210/pdb4z2c/pdb, to be published.
[31] A.K. Shiau, D. Barstad, P.M. Loria, L. Cheng, P.J. Kushner, D. A. Agard, G.L. Greene, The structural basis of estrogen receptor/coactivator recognition and the antagonism of this interaction by tamoxifen, Cell 95 (7) (1998) 927–937, https://doi.org/10.1016/S0092-8674(00)81717-1.
[32] N. Strushkevich, S.A. Usanov, H.-W. Park, Structural basis of human CYP51 inhibition by antifungal azoles, J. Mol. Biol. 397 (4) (2010) 1067–1078, https://doi.org/10.1016/j.jmb.2010.01.075.
[33] R.G. Kurumbail, A.M. Stevens, J.K. Gierse, J.J. McDonald, R. A. Stegeman, J.Y. Pak, D. Gildehaus, J.M. iyashiro, T.D. Penning, K. Seibert, P.C. Isakson, W.C. Stallings, Structural basis for selective inhibition of cyclooxygenase-2 by anti-inflammatory agents, Nature 384 (6610) (1996) 644–648, https://doi.org/10.1038/384644a0.
[34] C.A. Lipinski, F. Lombardo, B.W. Dominy, P.J. Feeney, Adv. Drug Deliv. Rev. 46 (2001) 3–26.
[35] A.D. Becke, Density-functional thermochemistry. III. The role of exact exchange, J. Chem. Phys. 98 (7) (1993) 5648–5652, https://doi.org/10.1063/1.464913.
[36] C. Lee, W. Yang, R.G. Parr, Development of the Colle-Salvetti correlation-energy formula into a functional of the electron density, Phys. Rev. B 37 (1988) 785–789.
[37] F. Weigend, R. Ahlrichs, Balanced basis sets of split valence, triple zeta valence and quadruple zeta valence quality for H to Rn: design and assessment of accuracy, Phys. Chem. Chem. Phys. 7 (18) (2005) 3297, https://doi.org/10.1039/b508541a.
[38] F. Neese, F. Wennmohs, A. Hansen, U. Becker, Efficient, approximate and parallel Hartree-Fock and hybrid DFT calculations. A 'chain-of-spheres' algorithm for the Hartree-Fock exchange, Chem. Phys. 356 (2009) 98–109.
[39] C. van Wüllen, Molecular density functional calculations in the regular relativistic approximation: Method, application to coinage metal diatomics, hydrides, fluorides and chlorides, and comparison with first-order relativistic calculations, J. Chem. Phys. 109 (2) (1998) 392–399, https://doi.org/10.1063/1.476576.
[40] E. vanLenthe, E.J. Baerends, J.G. Snijders, Relativistic regular two-component Hamiltonians, J. Chem. Phys. 99 (1993) 4597–4610.
[41] E. vanLenthe, E.J. Baerends, J.G. Snijders, Relativistic total energy using regular approximations, J. Chem. Phys. 101 (1994) 9783–9792.
[42] F. Neese, The ORCA program system, WIREs Comput Mol Sci 2 (1) (2012) 73–78, https://doi.org/10.1002/wcms.81.